DEVELOPMENT OF A WEST AND CENTRAL AFRICA REGIONAL VIDEO CAMERA NETWORK TO MONITOR COASTAL RESPONSE TO MULTISCALE OCEAN FORCING

Gregoire Abessolo Ondoa[1,2], Rafael Almar[2], Bruno Castelle[3], Magnus Larson[4], Minette Tomedi Eyango[1,5], Frédéric Bonou[6,7], Yves Du Penhoat[2,6,7], Ibrahima Camara[8], Moussa Sall[9], Raphaël Onguéné[10], Gael Alory[2,6,7]

Abstract

Incident wave conditions and morphological beach response in the region of West and Central Africa are investigated using data collected with a regional network of permanent video cameras systems. Daily beach profiles were computed combining video shoreline detection at different tide levels and bathymetric estimate from wave celerity at three specific sites: Grand Popo (Benin), Mbour (Senegal) and Kribi (Cameroon). Results show that the low tide terrace of the intermediate-reflective beach of Grand Popo affects shoreline response at the event and seasonal time scales by modulating wave energy at the beach face. Based on this preliminary study and in the framework of a sustainable video station deployment, this paper highlights the potential of a video station network to address waves and coastal response on the time scales from hours to decade(s) in tropical coastal environments where data are lacking.

Key words: shoreline, bathymetry, morphodynamics, regional climate, remote sensing, wave forcing

1. Introduction

Coastal vulnerability, defined as the susceptibility of a coastal area to be impacted by either inundation or erosion, affects the majority of world coastlines and results in the destruction of property and infrastructure (Gianluigi et *al.*, 2014, Tano et *al*., 2016). Understanding this coastal vulnerability remains a scientific challenge (Stive, 2004). Climate change drives sea-level rise and changes in storminess that will increase this vulnerability in coastal areas (Stive et *al*., 2002). Damage and losses associated with erosion and flooding also sometimes reflect absent or inadequate coastal management strategies due to a lack of understanding of coastal processes (Hoggart et *al.*, 2014, Nabil et *al.*, 2014). This is particularly true in developing countries where rampant anthropization increases coastal risks to people. Numerous studies show the significant impact of storms (Masselink et *al.*, 2015, Castelle et *al*., 2015,) and surge events (Quinn, 2014) on coastal areas, and the link between high frequency (short-term events, <30 days) and longer term (inter-annual) evolution has been investigated through equilibrium shoreline models (Splinter et *al*., 2014, Hanson et *al*., 2010). In developing countries, the sparse or the lack of available data sets and

---

[1] Laboratoire de Ressources Halieutiques (LRH), EDSFA, University of Douala, Cameroon. gregsolo55@yahoo.fr

[2] LEGOS (CNRS/CNES/IRD/Université de Toulouse), Toulouse, France rafael.almar@ird.fr gael.alory@legos.obs-mip.fr yves.du-penhoat@ird.fr

[3] EPOC (Université de Bordeaux/CNRS) Talence, France b.castelle@epoc.u-bordeaux1.fr

[4] Department Of Water Resources Engineering (DWRE), Lund University, Sweden magnus.larson@tvrl.lth.se

[5] ISH Yabassi, University of Douala, Cameroon, tomedi_tabi@yahoo.fr

[6] International Chair in Mathematical Physics and Applications/ Unesco Chair, University of Abomey-Calavi, Cotonou Benin, fredericbonou@yahoo.fr

[7] Institut de Recherches Halieutiques et Océanologiques du Bénin (IRHOB), Centre Béninois de la Recherche Scientifique et Technique, 03 BP 1665 Cotonou, Benin

[8] LPAO-SF/ESP, Université Cheikh Anta Diop, Sénégal ibrahima1.camara@ucad.edu.sn

[9] Centre de Suivi Ecologique (CSE), MOLOA, Sénégal, sall@cse.sn

[10] Institut Universitaire de Technologie (IUT) de Douala, University of Douala, Cameroon ziongra@yahoo.fr

suitable modeling tools, result on a multi-scale coastal evolution poorly known (Almar *et al.*, 2014). And it is even more pertinent in tropical coasts, characterized by a strong inter-annual variability and generally moderate average energy with energetic extreme events. In West and Central African regions in the Gulf of Guinea, coasts are exposed to the influence of energetic swells from the South Atlantic (southern hemisphere sub: 30:35°S, and extra-tropics: 45:60°S), modulated by the Southern Annular Mode (SAM) and locally generated short-crested waves, influenced by equatorial fluctuations of the local Inter-Tropical Convergence Zone (ITCZ) (Almar *et al.*, 2015, Laibi et al., 2014). Shimura *et al.* (2013) showed that the North Atlantic Oscillation (NAO), with maximum wave energy during austral summer period, is not the dominant mode for waves on the Sénégal coast (in the western part of West African region), also affected by South Atlantic dynamic. Beaches of this region are commonly microtidal, low-tide terraced with moderate energetic swell $H_S \sim$ 1–1.5 m. Miles at *al.* (2004) showed that the terrace/steep beach exhibit characteristics of dissipative/reflective sites. During low tide, large wave dissipation occurs along the full extension of the terrace, contrasting with high tide where waves dissipate most of their energy at the lower beach face. The low tide terrace protects the beach by dissipating wave energy further offshore and has therefore an impact on shoreline cross-shore response. This study suggested that shoreline evolution is influenced simultaneously by wave height in the breaking zone, water depth, and terrace width. Available literature concerning the evolution of the width of the terrace is still scarce. Understanding the dynamics of specific tropical Low Tide Terrace beaches is therefore of strong scientific interest that we address thereafter.

The wide range of scales of variability of coastal systems poses severe challenges to conventional in-situ instruments, which are limited with regard to data collection in both space and time. Instead, remote sensing approaches can provide high-frequency and high-resolution proxy information on beach changes on spatially extensive areas (Holmann and Stanley, 2007). Video imagery offers an attractive low-cost alternative for continuous long-term monitoring, particularly suited for developing countries. Video nearshore monitoring was largely developed during the last decades and now offers a wide coverage of many nearshore variables such as shoreline (Boak *et al.*, 2005, Almar *et al.*, 2012a, Osorio *et al.*, 2012), intertidal beach morphology (Uunk *et al.*, 2010, Osorio *et al.*, 2012), breaking wave height (Almar *et al.*, 2012b), wave celerity (Almar *et al.*, 2008), bathymetry (Almar *et al.*, 2011, Birrien *et al.*, 2013, Sembiring *et al.*, 2014, Bergsma *et al.*, 2016), and recently nearshore currents (Almar *et al.*, 2016a). Overall, Abessolo *et al.* (2016) suggested that video stations are efficient tools to monitor coastal processes at high frequency (minutes to hours) over the long term (years to decades), in complement to other conventional approaches, in the Gulf of Guinea. The potential of using such video systems was shown with a comparison between video and field measurements. A reasonable agreement was found for the significant wave height *Hs*, peak period *Tp*, direction, and beach profile, within the error range of existing methods (0.3-0.7 m reported in Plant and Kingston, 2007). The development of video systems along the coasts of Central and West Africa offers the possibility to describe regional oceanic forcing and coastal response at different pilot sites.

In this work, we investigate wave dynamics and beach response in the tropical sub-region of Central and West Africa using low-cost video stations and recent advances in processing video data. An analysis of the evolution of daily wave characteristics, shoreline positions, and bathymetric profiles is presented. This study includes a validation of intertidal and bathymetric beach profiles from video with field measurements followed by an analysis of 3.5 years of evolution of the terrace width at the Grand Popo site.

2. Methods

2.1. *Video systems and data*

This study focuses on the West and Central Africa region. Data used in this paper were collected continuously at 3 field sites with long-term low-cost video stations. Video stations consist of a camera collecting images at high frequency (2 Hz) and an on-site computer processing the raw images and storing three types of secondary images every 15 minutes: snapshot, cross-shore time stacks, and 15-min time-averaged images. Video stations are installed at (see Figure 1):
- Grand Popo (GPP), Benin, since February 2013, using a VIVOTEK IP 7361 camera (1600 x 728 pixels). This site is an intermediate-reflective, micro-tidal (from 0.3 to 1.8 m for neap and spring tidal ranges, respectively), wave-dominated (annual mean from ERAInterim $H_S \sim$1.4 m, $T_P \sim$9.4 s,

S-SW, RTR~1), medium grain-sized D_{50}=0.6 mm, alongshore uniform, low-tide terrace beach. This site is far enough from the influence of major towns, industrial areas, and harbours (Cotonou, 80 km and Lome, 60 km, respectively, in the down- and updrift directions). Some groyne fields were constructed 20 km updrift during 2015 with limited influence on Grand Popo.

- Mbour (MBR), Sénégal, since December 2014, using a VIVOTEK IP 7361 camera (1176 x 720 pixels). This site is micro-tidal (from 0.3 to 2 m for neap and spring tidal ranges, respectively), wave-dominated (annual mean from ERAInterim H_S~1.5 m, T_P~9.2 s, NW-SW, RTR~1), medium grain-sized D_{50}=0.4 mm, located 80 km south of Dakar, 5 km from the seaside Sally resort.
- Kribi (KRB), Cameroon, since May 2015, using a VIVOTEK IP 7160 camera (1600 x 1200 pixels). This site is an intermediate-reflective, micro-tidal (from 0.4 to 1.8 m for neap and spring tidal ranges, respectively), wave-dominated (annual mean from ERAInterim H_S~0.9 m, T_P~11s, SW, RTR~1), medium grain-sized D_{50}=0.5 mm, alongshore winding, rocky beach. This site is located in an urban area with high anthropogenic influence. A new deep water port has been constructed about 25 km upstream.

The ERAInterim hindcast data set of global meteorological variables (Sterl and Caires, 2005), generated by the ECMWF Wave Atmospheric Model WAM (The Wamdi Group, 1988), are used in this study.

On each study site, several ground control points were taken with GPS or DGPS (centimeter precision), including camera location. Geo-referencing and rectification of distortion (due to camera lens) of secondary images was accomplished using the direct linear transformation method (Holland *et al.*, 1997) applied to control points.

A 10-day field experiment was conducted at Grand Popo, Benin from 10 March to 19 March, 2014 (Abessolo *et al.*, 2016, Almar *et al.*, 2016b). Measurements included both sea and beach morphological surveys with Differential GPS and bathymetric sonar, while offshore forcing (waves and tide) was characterized using an Acoustic Doppler Current Profiler (ADCP) moored in 10-m depth.
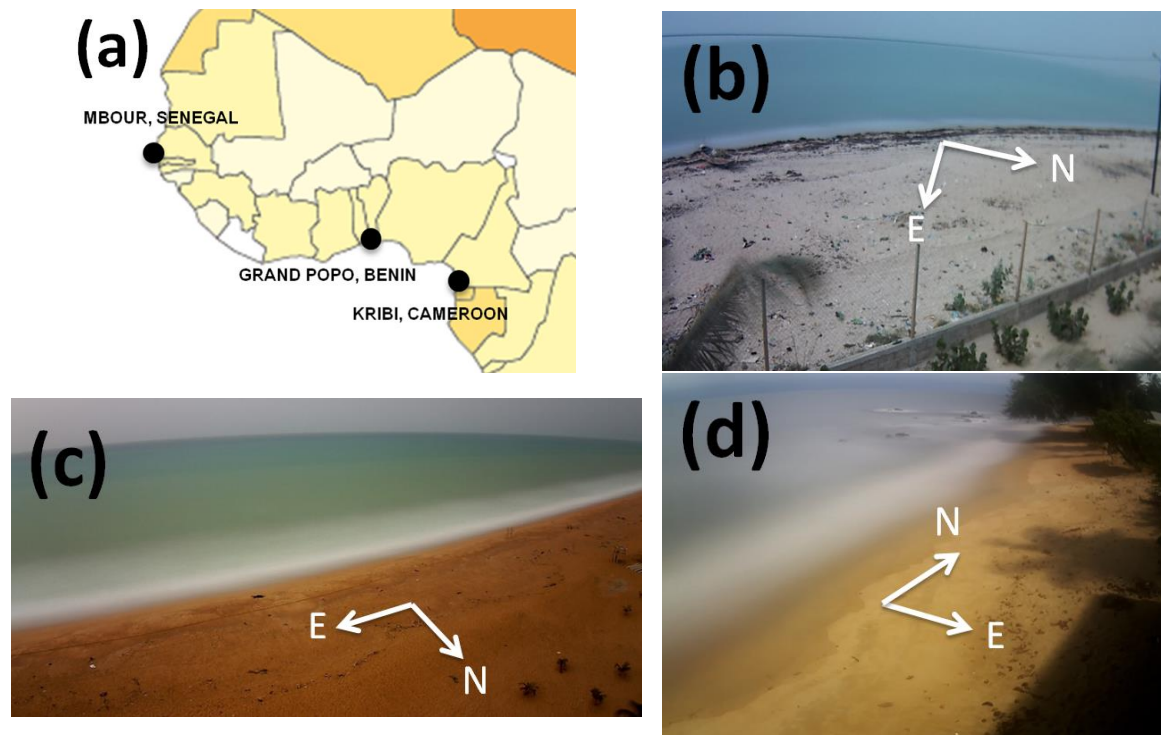
Figure 1. Video station locations in West and Central Africa (a) and 15-min video averaged images at Mbour (b), Grand Popo (c), and Kribi (d)

2.2. *Wave characteristics from video images*

Three wave characteristics are extracted in this study: H_S, mean period (T_m), and direction (*Dir*). The H_S video estimations are obtained from the cross-shore time stacks images using the method relying on the abrupt change of wave optical characteristics at the breakpoint (Almar *et al.*, 2012). Wave breakpoints are detected from the pixel intensity threshold. The pixel intensity peak, which appears at the wave crest, is calculated by the standard deviation of pixel intensity of each time series. This allows for tracking the change of intensity and for identifying the specific points with a sudden pixel intensity rise. The wave height can therefore be estimated as $H_S=(L_0-cor)tan(\beta)$ with the correction parameter $cor=L_0/(tan(\alpha_i))$ $tan(\beta)$, L_0 being the width of the crest, α_i the incident wave angle to the shore, and β the camera view angle.

T_m is computed from the offshore pixel intensity time series following the mean zero-crossing method detailed in Almar *et al*. (2008). Wave direction is estimated from the instantaneous and 15-minute averaged images. The technique consists of removing the averaged image from the instantaneous image (remove the background that does not move) and to highlight the wave crests (that move), then rectifying on a regular grid, and recovering the angle of the crest of the waves by the Radon transform (Almar *et al.*, 2013).

Video H_S and T_m data are regressed using field offshore forcing measurements (collected during the Grand Popo field measurements of March 2014 with an ADCP) for the case of Grand Popo site, or ERA-Interim hindcast data, generated by the ECMWF Wave Atmospheric Model WAM (The Wamdi Group, 1988) in the Atlantic Ocean, for the cases of Kribi, Cameroon and Mbour, Sénégal. These hindcast data were propagated from deep water to the breakpoint using Larson *et al*. (2010) formula.

2.3. *Automated shoreline delineation*

The approach adopted in this study is the MSV (Minimum Shoreline Variability) method (Almar *et al.*, 2012). The MSV method determines the shoreline location on time-averaged video images by combining two intrinsic shoreline properties: the color difference between water and sand and the presence of swash, not necessarily breaking. Beach pixels usually exhibit high red-channel (R) values and low green-blue-channel (*G-B*) values (i.e., high *R/G-B* ratios), whereas water pixels exhibit intense green-blue-channel values and low red-channel values (i.e., low *R/G-B* ratios). The *R/G-B* ratios are thus computed for all pixels within the region of interest. The local minimum, i.e., the transition zone between lower and higher *R/G-B* peaks associated with water and beach, respectively, is taken as a first estimate of the shoreline. Based on the physical fact that swash is always present at the shoreline, regardless of the complexity of the topography and the local occurrence of breaking, the shoreline is detected using the swash signature. Several contour lengths L are computed for different *R/G-B* values around the local minimum identified. L depends on the width of the region of interest and its variation ΔL is typically on the order of 1 to 30% of L. The local minimum of $\Delta L/L$ for varying *R/G-B* is used to infer the associated value of $R/G-B_{shoreline}$ and thus the contour position (*x, y*), while assuming that two close contours of *R/G-B* values at the shoreline have similar shapes. The identified shoreline on time-averaged images is converted to real-world coordinates using a rectification matrix obtained from the direct linear transformation method (Holland et al., 1997).

Determination of the intertidal beach profile involved the delineation of the shoreline at different tidal levels (Aarninkhof et al., 2003) and interpolation between low and high tides day by day. Sea level for the study period 2013-2016 was extracted from WXTide32 model, version 4.7. To reduce the longshore detection error, shoreline video positions were averaged alongshore.

2.4. *Celerity detection and automated bathymetric inversion*

First, time-stack images were pre-treated to clean up the wave intensity signal. A pass-band filter between 0.05 and 0.5 Hz was used to remove low-frequency (changing in light due to clouds) and high-frequency components (wind-waves or a rapid adjustment of the camera "auto-iris"). Then, the signal was normalized by dividing the intensity wave signal with the local intensity maximum (Almar et *al*., 2008).

Second, the wave spectrum on a time stack image was evaluated and the main components were extracted. For each spectral component f_i, the associated celerity C_{ij} for a position j on the cross-shore stack was estimated using the method presented by Almar *et al*. (2008) and Birrien *et al*. (2013), based on time-

and space-domain correlation. An arbitrary time lag *Δt=3 seconds* was fixed. For each position j, a time-domain cross-correlation R was computed with the neighboring position k from 1 to n, using the previously fixed $Δt$. The index with the maximum correlation gave an estimate of the time-integrated distance $Δx$ made by waves during $Δt$. Thus, we get a local estimate of the celerity as $C_{ij}=Δx/Δt$, corresponding to the spectral component f_i. By combining the celerities C_{ij}, an accurate estimate of the celerity was obtained. This was repeated for each of the positions i.

The bathymetric inversion scheme was based on the linear dispersion relation using video estimates of periods and celerities. This yielded estimates of the depth D_{ij} corresponding to the celerity C_{ij} for the spectral component f_i at a position j on the cross-shore stack. The local estimation of the depth D_j at the position j of the cross-shore stack was given by weighted averages of D_{ij}. The video depth estimates were regressed using field bathymetric surveys collected during the Grand Popo field measurements of March 2014 for the case of Grand Popo, Benin.

3. Results

3.1. *Wave characteristics and shoreline variability*

Figure 2 shows the monthly evolution of wave characteristics and shoreline position from video imaging for our study sites. At Grand Popo (GPP), Benin, 3.5-year processed data (February 2013 to May 2016) shows a well-observed variability of H_S and shoreline position (black dots), negatively correlated 73 %. High values of H_S (1.6 m), corresponding to the most eroded beach state, are obtained for the June-July-August period (JJA), including high energetic S-SW swells from the South Atlantic (average T_m of 10.2 s and wave incidence of 19 ° with respect to shore normal) and wind waves generated locally. An observed trend of decreasing H_S is captured (~ -0.1 m for the study period) as well as for wave direction (trend ~ -3°), see Abessolo et al., (2017).

At Kribi, Cameroon, 1-year processed data (May 2015 to May 2016) shows a maximum monthly H_S value of 1 m, obtained for the JJA period. Wave forcing estimates correspond to high energetic swell from the South Atlantic with an average monthly T_m of 9.5 s and a shore normal direction 6 °. Swell waves thus arrive with an incidence almost normal to the coast and the shoreline location seems to be positively correlated to H_S. Both H_S and shoreline position show a lower monthly variability comparing to Grand Popo.

At Mbour, Senegal, 11 months (December 2014 to October 2015) of video data were processed. A maximum monthly H_S value of 1.6 m was obtained in February with an average T_m of 9.5 s, and a shore normal wave direction of 24 °, corresponding to high energetic swells generated from the north Atlantic during austral summer period, that is, December-January-February (DJF). The H_S and shoreline position are positively correlated (60 %). Compared to Grand Popo and Kribi sites, wave direction and shoreline variability are more important. We can observe a change in wave direction between February and May.

3.2. *Bathymetric profile evolution at Grand Popo beach, Benin*

A validation of video-derived intertidal and bathymetric profiles is presented in Figure 3 for a 10-day field experiment conducted at Grand Popo, Benin from 10 March to 19 March, 2014. In Figure 3a, the principle of video intertidal beach reconstruction is illustrated, by interpolating shoreline location at different tide levels. These intertidal profiles were averaged over the validation period (Figure 3d, the blue line). The celerity extraction is illustrated in Figure 3b with the time-domain cross-correlation matrix R, previously averaged over the 10-day experiment, where a significant maximum correlation (>25 %) is observed for a cross-shore area between 75 and 175 meters from the location of the camera. The neighboring pixels (Interval in Figure 3b) of maximum correlation give the corresponding time-integrated distance $Δx$ made by the waves during $Δt$=3 s. The associated celerity of this maximum correlation is shown in Figure 3c. A root-mean-square error (RMSE) of 0.1 meters is obtained, implying a well estimated terrace shape with the video; see Figure 3d (red line). This video bathymetric estimation was smoothed over 20 meters for the cross-shore stack. The low-tide terrace is detected for a depth ~ 1 meter. The width of the terrace at Grand Popo, Benin can be considered as proportional to the distance between the shoreline location and the 1-meter depth contour.
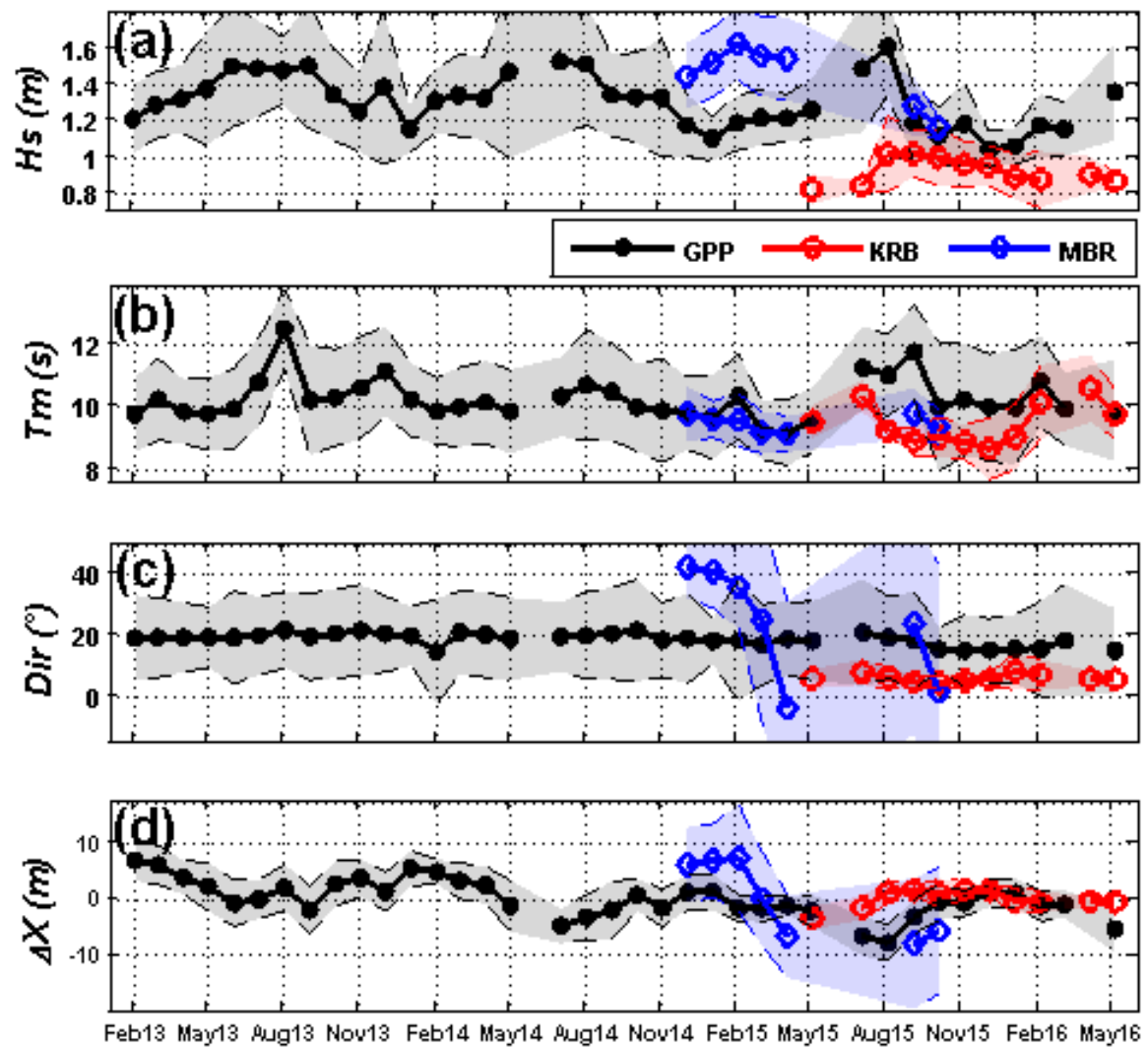
Figure 2. Monthly averaged video estimates (a) H_S, (b) T_m, (c) shore normal wave's direction and (d) shoreline variation around the average location, for the three study sites Grand Popo (GPP) in black dots, Kribi (KRB) in red circles and Mbour (MBR) in blue diamond-shaped. Shaded zones (black, blue and red) stand for day-to-day dispersion (standard deviation). Austral winter periods are in shaded yellow zones.
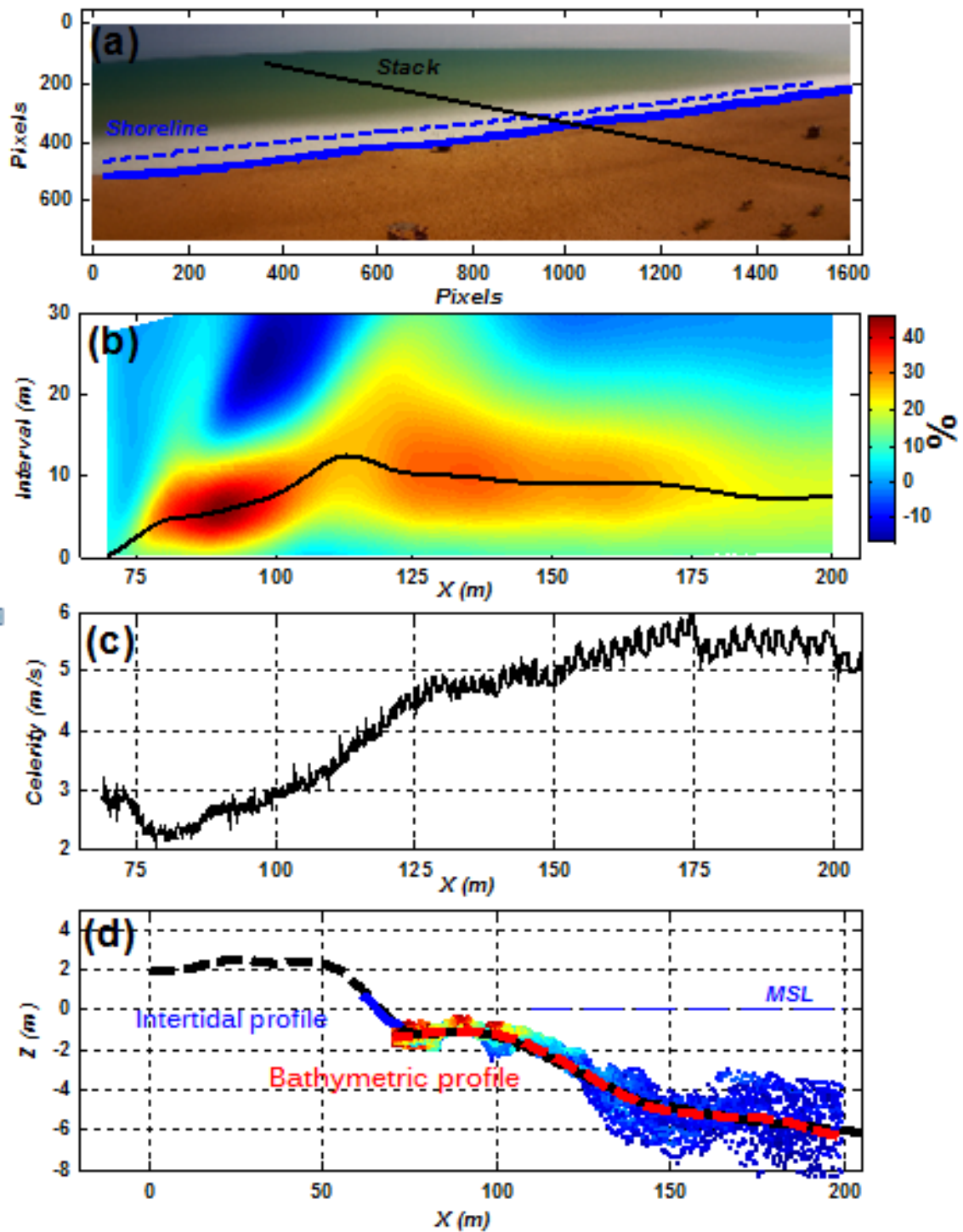
Figure 3. Validation of intertidal and bathymetric video profiles for the period of 10 to 19 March, 2014 at Grand Popo, Benin: (a) Shoreline detection on time-averaged images. Blue line is shoreline location for the presented image (high tide) and blue dashed line the shoreline location at low tide. Black line stands for the cross-shore stack for celerity detection (b) Matrix R of the correlation coefficients for each pixel X over the cross-shore stack from the beach to offshore. *Interval* represents the distance Δx (pixels) corresponding to the time lag $\Delta t=3$ seconds. The black line stands for the maximum correlation for the position X. (c) Video celerity estimation on the cross-shore stack (d) Comparison of video intertidal (blue) and bathymetric profiles (red) with data density colored and Grand Popo 2014 DGPS and bathymetric sonar (black). MSL stands for mean sea level.
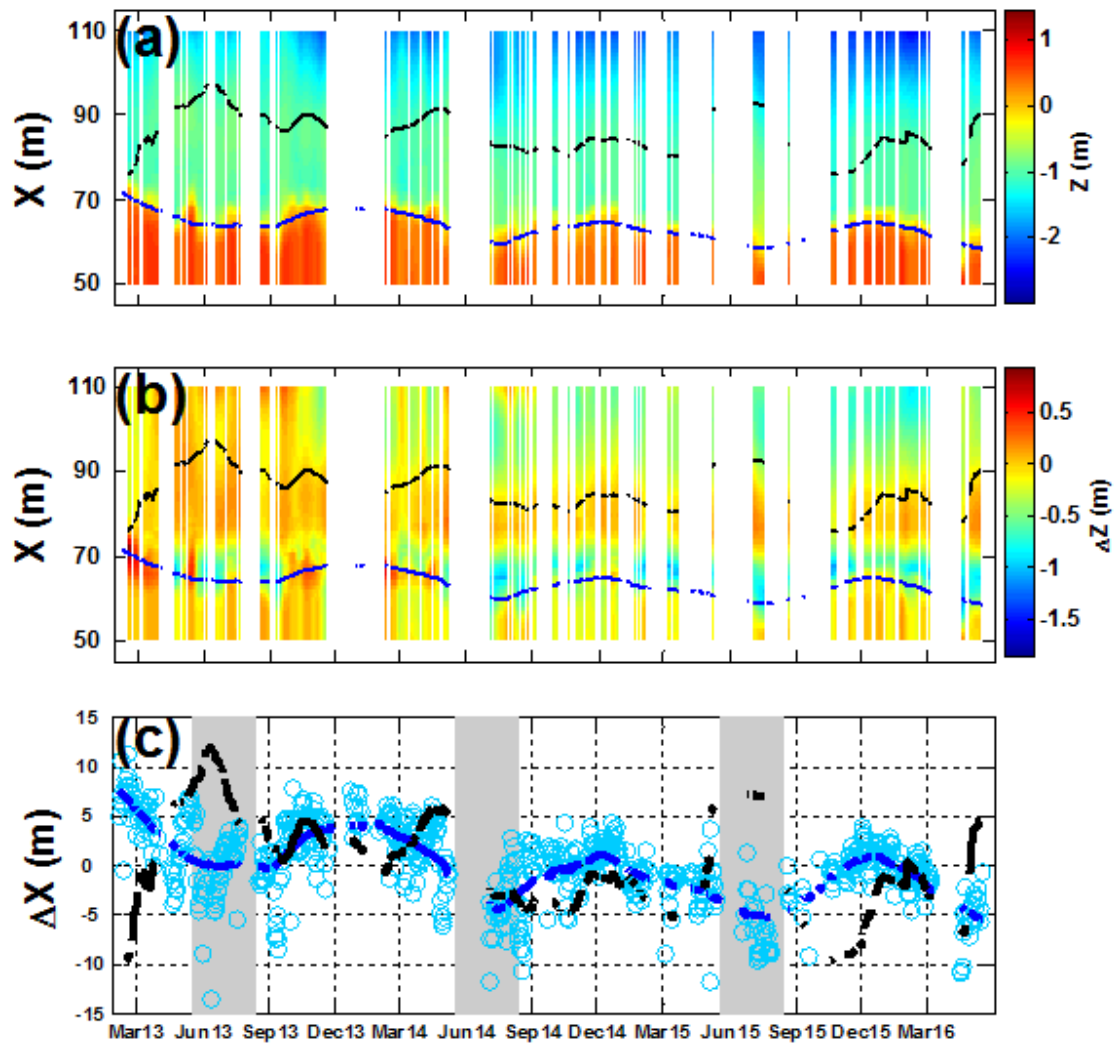
Figure 4. Video-derived profile evolution at Grand Popo, Benin: (a) Daily video intertidal and bathymetric profile evolution with regard to the position of the video camera. The black line stands for the end of the terrace (depth equal to 1 meter) and the blue line stands for the shoreline location. These lines were smoothed over 30 days. (b) Perturbation of daily beach profiles. This perturbation is computed by removing the initial beach profile from each daily profile. (c) Evolution of daily position of the end of the terrace (black line) and daily shoreline location (blue line) with austral winter period in grey. For each variable, data ΔX are obtained by removing the average position. Solid lines are smoothed over 30 days. Blue circles are daily shoreline location.

The video system installed at Grand Popo beach collects time-averaged and time stack images every 15 minutes. Daily intertidal video profiles are computed with shoreline detection on time-averaged images and daily bathymetric profiles are obtained by averaging 15-min bathymetric profiles, computed from each time stack image. Using the validation presented on Figure 3, the maximum of time-domain cross-correlation matrix R better than 25 % is observed for cross-shore area between 75 and 175 meters from the location of the camera. Grand Popo terrace is located between 75 and 100 meters, as observed during field measurements. An overall profile of the beach, combining intertidal and bathymetric profiles, is reconstructed for a cross-shore distance of 60 meters, corresponding to the area between 50 and 110 meters from camera location (see Figures 4). Beyond the influence of waves, offshore bathymetry (depth below 3 meters) is considered as unmoved. Daily profiles were smoothed over 15 consecutive days.

In Figure 4a, the location of the shoreline and the end of the terrace (depth equal to 1 meter) show substantial event and inter-annual variability. Grand Popo beach presents an average distance from shoreline to end of terrace (depth equal to 1 meter below MSL) of 18 m, with minimum 15 m and maximum 22 m. The terrace is located at 65-100 m from the camera location. Figure 4b shows the perturbation of the beach profile, computed by removing the initial profile from each daily beach profile. Two erosive perturbations can be observed regarding the location of the shoreline and the end of the terrace, respectively, ~60 m and ~100 m from camera location. These perturbations are also observed in Figure 4c on the inter-annual scale with, respectively -0.3 m/year for shoreline position and -0.2 m/year for the position of the end of the terrace, for the study period 2013 to 2016. By removing respective trends, a negative correlation of 41 % is obtained at the monthly scale. During the erosive phase June-July-August (JJA) the width of the terrace seems to increase, whereas it decreases during accretive phase December-January-February (DJF).

Looking in Figures 2 and 4, the terrace width is small during the austral summer period (December-January-February) when wave energy is low, while it is large during the winter period (June-July-August) when wave energy is high. The erosive shoreline phase therefore corresponds to an accretive terrace phase and the accretive shoreline phase corresponds to an erosive terrace phase.

4. Conclusion

Regarding the regional wave climate in West and Central Africa, important morphological beach changes occur with high wave energy conditions, corresponding to H_S values. The region is under the influence of both north and south Atlantic climate dynamics and local generated wind-waves, leading to such different responses in the coastal environments as observed in this study. Kribi beach is less affected by energetic swells, coming from the South Atlantic, modulated by SAM (average H_S ~0.9 m), but terrace width seems to be similar to Grand Popo. Seasonal shoreline variation is the smallest compared to Grand Popo and Mbour. The Mbour site presents a typical impact of both north and south Atlantic forcing, with important changes in the wave direction. However, this needs to be confirmed by field measurements. Grand Popo site is characterized by a typical H_S–terrace width configuration, leading to a particular variability in shoreline position. The regional network installed in West and central Africa is therefore important for monitoring both hydrodynamic and near-shore morphological process.

The temporal correlations between three parameters derived from video image analysis were investigated at Grand Popo, Benin with the following result: H_S and shoreline position was negatively correlated and the shoreline position was also negatively correlated with the position of the end of the terrace, therefore to the terrace width as well. When high energetic wave conditions occurs (June-July-August period for Grand Popo), the wave energy combined with the sea level are sufficient to induce beach-face erosion and the retreat of the shoreline. An increase of the terrace width is observed, probably due to eroded sediment (from the beach face) that is trapped between the incident waves and the swash zone. This leads to a wider dissipative surf zone. When incident wave energy decreases, dissipation occurs along the extension of the terrace. The shoreline moves offshore due to onshore transport sediments from the terrace, resulting in a decreasing of terrace width. During austral winter (June-July-August), the shoreline retreat is even more significant at high tide when the beach face is most affected. These observations indicate the effect of terrace on event and seasonal scales in a typical intermediate to reflective beach as Grand Popo.

Acknowledgements

References

Abessolo Ondoa, G., Almar, R., Kestenare, E., Bahini, A., Houngue, G. H., Jouanno, J., Du Penhoat, Y., Castelle, B., Melet, A., Meyssignac, B., Anthony, E. J., Laibi, R., Alory, G., Ranasingue, R., 2016. Potential of Video Cameras in Assessing Event and Seasonal Coastline Behaviour: Grand Popo, Benin (Gulf of Guinea). *Journal of Coastal Research*, SI 75: 442-446.

Abessolo Ondoa, G., Bonou, F., Tomety, F. S., Du Penhoat, Yves, Perret, C., Degbe, C. G. E., Almar, R., 2017. Event to seasonal and inter-annual coastal evolution at Grand Popo, Benin. *Water*, (submitted).

Almar, R., Senechal, N., Bonneton, P., Roelvink, J. A., 2008. Wave celerity from video imaging: validation with in-situ Pre-ECORS data. *Proc. I. C. C. E.* 1 (5), 661–673.

Almar, R., Cienfuegos, R., Catalán, P. A., Birrien, F., Castelle, B. and Michallet, H., 2011. Nearshore bathymetric inversion from video using a fully non-linear Boussinesq wave model. *Journal of Coastal Research*, SI 64: 20 – 24.

Almar, R., Ranasinghe, R., Catalan, P. A., Senechal, N., Bonneton, P., Roelvink, D., Bryan, K. R., Marieu, V., and Parisot J. P., 2012a. Video-based detection of shorelines at complex meso-macro tidal beaches. *Journal of Coastal Research*, 28(5): 1040-1048.

Almar, R., Cienfuegos, R., Catalan, P. A., Michallet, H., Castelle, B., Bonneton, P., and Marieu, V., 2012b. A new breaking wave height direct estimation from video. *Coastal Engineering*, 61: 42-48.

Almar, R., Bonneton, P., Michallet, H., Cienfuegos, R., Ruessink, G. and Tissier, M., 2013. On the use of the radon transform in studying nearshore wave dynamics. *Coastal Dynamics* 2013, 73-82.

Almar, R., Honkonnou, N., Anthony, E. J., Castelle, B., Senechal, N., Laibi, R., Mensah-Senoo, T., Degbe, G., Quenum, M., Dorel, M., Chuchla, R., Lefebvre, J. P., Du Penhoat, Y., Laryea, W. S., Zodehougan, G., Sohou, Z., Addo, K. A., Ibaceta, R., Kestenare, E., 2014. The Grand Popo beach 2013 experiment, Benin, West Africa: from short timescale processes to their integrated impact over long-term coastal evolution. *Journal of Coastal Research*, SI 70, 651-656.

Almar, R., Kestenare, E., Reyns, J., Jouanno, J., Anthony, E.J., Laibi, R., Hemer, M., Du Penhoat, Y., Ranasinghe, R., 2015. Response of the Bight of Benin (Gulf of Guinea, West Africa) coastline to anthropogenic and natural forcing, Part1: Wave climate variability and impacts on the longshore sediment transport. *Continental Shelf Research*, Vol 110, 48-59.

Almar, R., Larnier, S., Castelle, B., Scott, T., Floc'h, F., 2016a. On the use of the Radon transform to estimate longshore currents from video imagery. *Coastal Engineering*, 114: 301–308.

Almar, R., Almeida, P., Blenkinsopp,C., and Catalan, P., 2016b. Surf-swash interactions on a low-tide terraced beach. *Proceedings of the 14th International Coastal Symposium* (Sydney, Australia). Journal of Coastal Research, Special Issue, 75, 348-352.

Angnuureng, D. B., Almar, R., Addo, K. A., Castelle, B., Senechal, N., Laryea, S. W., Wiafe, G., 2016. Video Observation of Waves and Shoreline Change on the Microtidal James Town Beach in Ghana. *Journal of Coastal Research*, SI 75: 1022-1026.

Aarninkhof, S.G. J.; Turner, I.L.; Dronkers, D.T.; Caljouw, M. and Nipius, L., 2003. A video-base technique for mapping intertidal beach bathymetry. *Coastal Engineering*, 49 (4), 275–289

Ba, A. and Senechal, N., 2013. Extreme winter storm versus Summer storm: morphological impact on a sandy beach. *Journal of Coastal Research*, SI 65: 648-653.

Bergsma, E.W.J., Conley, D.C., Davidson, M.A. and O'Hare, T.J., 2016. Video-based nearshore bathymetry estimation in macro-tidal environments. *Marine Geology*, 374: 31–41.

Birrien, F., Castelle, B., Marieu, V., Dubarbier, B., 2013. On adata-model assimilation method to inverse wave-dominated beach bathymetry using heterogeneous video-derived observations. *Ocean Engineering*, 73: 126–138.

Boak, E. H., Turner, I. L, 2005. Shoreline Definition and Detection: A Review. *Journal of Coastal Research*, 21(4): 688-703.

Castelle, B., Marieu, V., Bujan, S., Splinter, K. D., Robinet, A., Sénéchal, N., Ferreira, S., 2015. Impact of the winter 2013–2014 series of severe Western Europe storms on a double-barred sandy coast: Beach and dune erosion and megacusp embayments. *Geomorphology*, 238, 135–148.

Di Paola, G., Aucelli, P. P. C., Benassai, G., Rodriguez, G., 2014. Coastal vulnerability to wave storms of Sele littoral plain (southern Italy). *Nat Hazards,* 71:1795–1819.

Hanson, H., Larson, M., Kraus, N. C., 2010. Calculation of beach change under interacting cross-shore and longshore processes. *Coastal Engineering* 57, 610–619. doi:10.1016/j.coastaleng.2010.02.002

Hoggart, S.P.G., Hanley, M.E., Parker, D.J., Simmonds, D.J., Bilton, D.T., Filipova-Marinova, M., Franklin, E.L., Kotsev, I., Penning-Rowsell, E.C., Rundle, S.D., Trifonova, E., Vergiev, S., White, A.C., Thompsona, R.C., 2014. The consequences of doing nothing: The effects of seawater flooding on coastal zones. *Coastal Engineering*, 87: 169–182.

Holland, K. T., Holman, R.A. and Lippmann, T.C., 1997. Practical use of video imagery in near-shore oceanographic field studies. IEEE J. *Oceanic Engineering*, 22(1): 81-92.

Holman, R.A. and Stanley, J., 2007. The history and technical capabilities of Argus. *Coastal Engineering*, 54: 477–491.

Laibi, R., Anthony, E., Almar, R., Castelle, B., Senechal, N., Kestenare, E., 2014. Longshore drift cell development on the human-impacted Bight of Benin sand barrier coast, West Africa. *Journal Of Coastal Research*, SI 70, 78-83.

Larson, M., Hoan, L. X., Hanson, H., 2010. Direct formula to compute wave height and angle at incipient breaking. *Journal of Waterway, Port, Coastal and Ocean Engineering*, 136/2, 119-122.

Masselink, G., Scott, T., Russel, P., Davidson, M. A., Conley, D. C., 2015. The extreme 2013/2014 winter storms: hydrodynamic forcing and coastal response along the southwest coast of England. *Earth Surface Processes and Landforms*.

Osorio, A.F., Medina, R., Gonzalez, M., 2012. An algorithm for the measurement of shoreline and intertidal beach profiles using video imagery: PSDM. *Computers and Geosciences*, 46: 196–207.

Plant, N.G., Aarninkhof, S.G.J., Turner, I.L., and Kington, K.S., 2007. The performance of shoreline detection models applied to video imagery. *Journal of Coastal Research*, 23(3), 658–670

Postacchini, M. and Brocchini, M., 2014. A wave-by-wave analysis for the evaluation of the breaking-wave celerity. *Applied Ocean Research*, 46: 15–27.

Quinn, N., Lewis, M., Wadey, M. P. and Haigh, I. D., 2014. Assessing the temporal variability in extreme storm-tide time series for coastal flood risk assessment. *Journal of Geophysical Research: Oceans*, 119: 4983–4998, doi:10.1002/2014JC010197.

Sembiring, L., Dongeren, A., Winter, G., Ormond, M., Briere, C. and Roelvink, D., Nearshore bathymetry from video and the application to rip current predictions for the Dutch Coast. *Proceedings 13th International Coastal Symposium (Durban, South Africa), Journal of Coastal Research*, Special Issue No. 70: 354-359, ISSN 0749-0208.

Senechal, N., Coco, G., Castelle, B. and Marieu, V., 2015. Storm impact on the seasonal shoreline dynamics of a meso- to macrotidal open sandy beach (Biscarrosse, France). *Geomorphology*, 228: 448–461.

Shimura, T., Mori, N. and Mase, H., 2013. Ocean Waves and Teleconnection Patterns in the Northern Hemisphere. *Journal Of Climate*, 26, 8654-8670. DOI: 10.1175/JCLI-D-12-00397.1

Splinter, K. D., Turner, I. L., Davidson, M. A., Barnard, P., Castelle, B. and Oltman-Shay, J., 2014, A generalized equilibrium model for predicting daily to inter-annual shoreline response. *Journal Of Geophysical Research*, Earth Surf., 119, 1936–1958, doi:10.1002/2014JF003106.

Sterl, A., Caires, S., 2005. Climatology, variability and extrema of ocean waves– the web-based KNMI/ERA-40 Wave Atlas. *International Journal Climatology* 25, 963–977.

Stive, M. J. F., Aarninkhof, S. G. J., Hamm, L., Hanson, H.,Larson, M., Wijnberg, K. M., Nicholls, R. J., Capobianco, M., 2002. Variability of shore and shoreline evolution. *Coastal Engineering* 47, 211-235..

Stive,M., 2004.How important is global warming for coastal erosion? *Climate Change*, 64, 27–39.

Tano, R.A., Aman, A., Kouadio, K.Y., Toualy, E., Ali, K.E. and Assamoi, P., 2016. Assessment of the Ivorian Coastal Vulnerability. *Journal Of Coastal Research*, 32, 6, 1495–1503.

The Wamdi Group, 1988. The WAM model- a third generation ocean wave prediction model. *Journal of Physical Oceanography*, 18, 1775–1810.

Touili, N., Baztan, J., Vanderlinden, J. P., Kane I. O., Diaz-Simal, P., Pietrantoni, L., 2014. Public perception of engineering-based coastal flooding and erosion risk mitigation options: Lessons from three European coastal settings. *Coastal Engineering*, 87: 205–209.

Uunk, L., Wijnberg, K.M., Morelissen, R., 2010. Automated mapping of the intertidal beach bathymetry from video images. *Coastal Engineering*, 57: 461–469.